JOURNAL OF THERMOPHYSICS AND HEAT TRANSFER
Vol. 10, No. 4, October–December 1996

Turbine Blade Heat Transfer Prediction in Flow Transition Using k-ω Two-Equation Model

R.-J. Yang* and W.-J. Luo†
National Cheng Kung University, Tainan, Taiwan 701, Republic of China

The proper design of a turbine blade has an important effect on engine performance and efficiency. The thermal design of a turbine blade is also greatly influenced by the flow transition phenomena of the boundary layer. Transition in turbine flowfields is a complex process and is influenced by the Reynolds number, pressure gradient, geometry, and freestream turbulence, etc. In this study, a k-ω turbulence model is used to investigate the flow transition as well as problems concerned with heat transfer. The model predicts well the transition point and the associated transitional heat transfer coefficients for flat plate flows. With a suitable surface curvature correction to closure coefficients of the model, reasonable heat transfer predictions in flow transition are simulated for turbine blade flows.

Nomenclature

L = characteristic length scale
P = static pressure
Re = Reynolds number, $U_\infty L/\upsilon$
R_β, R_k, R_ω = closure coefficients in viscous damping functions
U_∞ = characteristic velocity scale
u_i = Cartesian velocity components
α, α^* = closure coefficients
α_0, α_0^* = closure coefficients in viscous damping functions
β, β^* = closure coefficients
γ = specific heat ratio
ρ = mass density
σ, σ^* = closure coefficients
τ_{ij} = Reynolds stress tensor
υ = kinematic molecular viscosity, μ/ρ

I. Introduction

AN important factor in the overall design of advanced gas turbine engines for propulsion technology focuses upon the flow in and about turbine blade passages. These components are the source of aerodynamic loads and losses that can control the overall machine efficiency and may be subject to extreme heat transfer problems. Improper estimates of loss coefficients may lead to inaccurate predictions of engine performance. Improper estimates of heat transfer rates may lead to poor component life and even catastrophic failure of components. One of the most significant factors affecting the accurate prediction in loss and heat transfer is boundary-layer transition. Transition phenomena from laminar to turbulent flow may be classified in two categories:

1) *Natural transition.* In a low freestream turbulence environment, the transition is caused by the amplification of Tollmien–Schlichting waves. The evolution of these waves leads to the development of three-dimensional unstable flows and eventual breakdown. Turbulent spots are produced following the breakdown of the waves, which are precursors of the fully turbulent boundary layer.

2) *Bypass transition.* In a high freestream turbulence environment, without the process of the two-dimensional Tollmien–Schlichting waves and three-dimensional unstable flows in natural transition, turbulent spots are formed directly in the boundary layer. In other words, the flow transition is because of the transport of turbulence from the freestream to the boundary layer, rather than from the amplification of Tollmien–Schlichting waves. Boundary-layer transition in turbine blades belongs to the second category. Theoretically, such a phenomenon can be simulated by direct numerical simulation (DNS). Because of the fact that immense grid points and computational time are required, it is not possible to apply the DNS to the current engineering analysis. To analyze engineering problems economically, we propose using physical modeling to study the transition phenomena.

Remarkable progress has been made in computational fluid dynamic (CFD) technology. Many researchers have developed efficient programs to calculate pressure distributions on turbine blades.[1–6] Nevertheless, owing to a lack of reliable transition models, such simulations almost neglect the boundary-layer transition. Effects of heat transfer are rarely taken into account. The often-used Baldwin–Lomax and k-ε models are employed to simulate fully turbulent flows. Some researchers have also tried to adopt these models to explore boundary-layer transition. For instance, Dorney and Davis[1] and Boyle[7] used the Baldwin–Lomax model to probe boundary-layer transition. However, the location of the transition point must be specified in advance. Not requiring the onset point to be known a priori, the k-ε model is adopted to study the transition phenomena by Schmidt and Patankar[8] and Yang et al.,[5] and yet modifications to the model are required.

Recently, Wilcox[9] has made a detailed analysis and comparison between the k-ε and k-ω models. In his calculations for 16 flows, he concludes that the k-ω model performs more accurately than the k-ε model. This is especially true for adverse pressure gradient flows. The k-ω model is rarely used to study boundary-layer transition phenomena for turbine blade flows. In this study, we solve the Navier–Stokes equations and k-ω model numerically to investigate turbine cascade flows as well as making comparisons between the results obtained by k-ω and Baldwin–Lomax models. The objectives are to study boundary-layer transition phenomena, and to make the physical modeling become a practical means for predicting aerodynamic losses and heat transfer accurately.

Received Nov. 6, 1995; revision received April 10, 1996; accepted for publication April 15, 1996.

*Associate Professor, Department of Engineering Science. Senior Member AIAA.
†Graduate Student, Department of Engineering Science.

II. Theoretical Analysis

A. Governing Equations

After taking Favre-averaging, the two-dimensional compressible Navier–Stokes equation can be written as follows.

Continuity equation:

$$\frac{\partial \rho}{\partial t} + \frac{\partial}{\partial x_j}(\rho u_j) = 0 \tag{1}$$

Momentum equation:

$$\frac{\partial}{\partial t}(\rho u_i) + \frac{\partial}{\partial x_j}(\rho u_i u_j + \delta_{ij} p - \hat{\tau}_{ij}) = 0 \tag{2}$$

Energy equation:

$$\frac{\partial}{\partial t}(e) + \frac{\partial}{\partial x_j}[(e + p)u_j + \overline{\rho u_j' h'} - q_j - u_i \hat{\tau}_{ij}] = 0 \tag{3}$$

where

$$h = \bar{e} + p/\rho, \quad \bar{e} = \frac{p}{[(\gamma - 1)\rho]}, \quad e = \rho[\bar{e} + 0.5(u^2 + v^2)]$$

$$\hat{\tau}_{ij} = 2\mu\left(S_{ij} - \frac{1}{3}\frac{\partial u_k}{\partial x_k}\delta_{ij}\right) + \tau_{ij}, \quad S_{ij} = \frac{1}{2}\left(\frac{\partial u_i}{\partial x_j} + \frac{\partial u_j}{\partial x_i}\right)$$

$$q_j = \gamma \mu Pr^{-1} \frac{\partial}{\partial x_j}(\bar{e})$$

$$\tau_{ij} = -\overline{\rho u_i' u_j'} = \mu_T\left(\frac{\partial u_i}{\partial x_j} + \frac{\partial u_j}{\partial x_i} - \frac{2}{3}\delta_{ij}\frac{\partial u_k}{\partial x_k}\right) - \frac{2}{3}\delta_{ij}\rho k$$

$$-\overline{\rho u_j' h'} = \mu_h \frac{\partial h}{\partial x_j}, \quad \text{and} \quad \mu_h = \frac{\mu_T}{Pr_t}$$

The molecular viscosity and conductivity are calculated from Sutherland's law. All flows computed in this study are airflows. The commonly used values for the laminar Prandtl number $Pr = 0.72$ and turbulent Prandtl number $Pr_t = 0.9$ for air are used here.

The Wilcox[10] k-ω two-equation turbulence model is governed by the following.

Turbulent kinetic energy equation:

$$\frac{\partial(\rho k)}{\partial t} + \frac{\partial(\rho k u_j)}{\partial x_j} = \tau_{ij}\frac{\partial u_i}{\partial x_j} - \beta^* \rho k \omega + \frac{\partial}{\partial x_j}\left[(\mu + \sigma^* \mu_T)\frac{\partial k}{\partial x_j}\right] \tag{4}$$

Specific dissipation rate equation:

$$\frac{\partial(\rho\omega)}{\partial t} + \frac{\partial(\rho\omega u_j)}{\partial x_j} = \alpha\frac{\omega}{k}\tau_{ij}\frac{\partial u_i}{\partial x_j} - \beta\rho\omega^2 + \frac{\partial}{\partial x_j}\left[(\mu + \sigma\mu_T)\frac{\partial \omega}{\partial x_j}\right] \tag{5}$$

and the eddy viscosity is $\mu_T = \rho k/\omega$. The closure coefficients are $\alpha = 5/9$, $\beta = 3/40$, $\beta^* = 9/100$, $\sigma = 1/2$, and $\sigma^* = 1/2$.

This k-ω model (henceforth called the original model) predicts flow transition to turbulence at Reynolds numbers that are too low. Wilcox[10] makes the following modifications to the model (henceforth called the modified model):

$$\mu_T = \alpha^* \frac{\rho k}{\omega}, \qquad \alpha^* = \frac{\alpha_0^* + Re_T/R_k}{1 + Re_T/R_k}$$

$$\alpha = \frac{5}{9}\cdot\frac{\alpha_0 + Re_T/R_\omega}{1 + Re_T/R_\omega}\cdot(\alpha^*)^{-1}$$

$$\beta^* = \frac{9}{100}\cdot\frac{5/18 + (Re_T/R_\beta)^4}{1 + (Re_T/R_\beta)^4}, \qquad \beta = \frac{3}{40}, \qquad \sigma^* = \sigma = \frac{1}{2}$$

$$\alpha_0^* = \frac{\beta}{3}, \qquad \alpha_0 = \frac{1}{10}, \qquad R_\beta = 8, \qquad R_k = 6, \qquad R_\omega = \frac{27}{10}$$

The quantity Re_T is the turbulence Reynolds number defined by

$$Re_T = \rho k/\mu\omega$$

B. Boundary Conditions

1. Boundary Conditions of the Two-Dimensional Navier–Stokes Equations

For subsonic flow conditions, characteristic analysis requires three inflow quantities and one outflow quantity to be specified. Currently, the total pressure, the Riemann invariant corresponding to the right running characteristic, and the inflow angle, are specified at the inlet. And the Riemann invariant corresponding to the left running characteristic is extrapolated from the interior of the inlet boundary. At the exit, the static pressure is specified, and three other variables are extrapolated from the interior. No-slip and adiabatic or isothermal conditions are applied at the solid surface. Periodic conditions are applied to simulate the effect of other blades.

2. Boundary Conditions of the k-ω Model

At the wall $k = 0$. The boundary condition of ω is based on the Wilcox[10] suggestion that

$$\omega = (u_\tau^2/\upsilon)S_R, \qquad y \to 0$$

where

$$u_\tau = \sqrt{\left(\frac{\upsilon \partial u}{\partial y}\right)_w}, \qquad S_R = \begin{bmatrix} \left(\frac{50}{k_R^+}\right)^2, & \text{if} \quad k_R^+ < 25 \\ \frac{100}{k_R^+}, & \text{if} \quad k_R^+ \geq 25 \end{bmatrix}$$

$k_R^+ = u_\tau k_R/\upsilon$, k_R is the average height of sand-grain roughness elements. In this study, we assume that the surface of the turbine blade is relatively smooth. In other words, the roughness height is very small. Following Wilcox,[10] k_R^+ has to be smaller than 5 to simulate a smooth surface. We use $(k_R^+)^2 = 1.25$ in these calculations.

At the exit and outer boundaries. The Neumann condition is used, in which $\partial\phi/\partial \boldsymbol{n} = 0$, $\boldsymbol{n}$ is the unit vector normal to the outer boundary, and ϕ represents k or ω.

At the inlet. We specify physical quantities of k_∞ and ω_∞. The k_∞ quantity can be obtained by converting the freestream turbulence intensity Q_{tur} from experimental data, i.e., $k_\infty/U_\infty^2 = 1.5Q_{\text{tur}}$. The ω_∞ can be thought of as an averaged frequency of the freestream turbulence. However, it is unclear how the freestream value of ω_∞ should be specified. We assume that the freestream is a homogeneous and isotropic turbulent field, the ω equation simplifies to

$$\frac{d\omega_\infty}{dt} = -\beta\omega_\infty^2$$

One can find the solution for ω_∞ given as

$$\omega_\infty \sim (1/\beta t)$$

where $\beta = 3/40$. Therefore, with a suitable time scale L/U_∞, $\omega = \mathbb{O}(10U_\infty/L)$. This is consistent with Menter's suggestion.[11]

C. Grid System and Solution Procedure

A multizone grid system has been adopted. The grid system chosen for the two-dimensional turbine blade consists of two different zones, namely, an inner O grid and an outer H grid. The inner grid encloses the turbine blade surface and accurately resolves the leading and trailing edges. The inner O grid is generated using an elliptic grid generator with the condition that the grid be orthogonal to the blade surface. The outer H grid is generated algebraically. Note that the H grid is constructed with the requirement that the metric coefficients be continuous across the periodic lines where periodic boundary conditions are applied.

The viscous effects are confined to the region close to the blade surface. The flow of the inner O grid zone is solved by the Navier–Stokes equations, and that of the outer H grid zone by the Euler equations. The turbulent eddy viscosity of the Navier–Stokes equation is provided by solving the k-ω two-equation models. The turbulence model equations are uncoupled from the mean flow equations during the solution process. The grid of the outer H grid zone exists concurrently with the grid of the inner O grid zone. Information transfer from the inner zone to the outer zone takes place at the inner zone overlap boundary. Information transfer between the different zones is effected by proper imposition of interface boundary conditions. Additional details regarding the implementation of zonal boundary conditions can be found in Rai.[12]

III. Numerical Algorithm

The Navier–Stokes equations in the O grid zone, and the Euler equation in the H grid zone are solved. The governing equations are cast in the strong conservation form written in the generalized curvilinear coordinate system. The numerical procedure used to solve the governing equations is an iterative, factored, implicit scheme. The method can be outlined as follows. The governing equations are replaced by a fully implicit finite difference approximation. Numerical fluxes are evaluated by the third-order-accurate upwind-biased Osher scheme.[13] Central differencing is used to evaluate all diffusion terms. The resulting system of nonlinear equations is solved by the Newton–Raphson iteration technique. To solve these equations at each iteration level, an approximate factorization method is used. This technique leads to a system of coupled linear difference equations with narrow block-banded structures that can be solved efficiently by a LU decomposition method.

The k-ω equations provide the turbulent eddy viscosity to be used in the Navier–Stokes equations. The numerical procedure is discussed briefly as follows. The physical quantities in k-ω equations are nondimensionalized and written in a generalized curvilinear coordinate (ξ, η) as

$$\frac{\partial \hat{Q}_t}{\partial \tau} + \frac{\partial \hat{E}_t}{\partial \xi} + \frac{\partial \hat{F}_t}{\partial \eta} - Re^{-1}\left(\frac{\partial \hat{E}_{tv}}{\partial \xi} + \frac{\partial \hat{F}_{tv}}{\partial \eta}\right) = \hat{H}_t \qquad (6)$$

where

$$\hat{Q}_t = J^{-1}\begin{bmatrix}\rho k \\ \rho\omega\end{bmatrix}, \qquad \hat{E}_t = J^{-1}\begin{bmatrix}(\xi_x u + \xi_y v)\rho k \\ (\xi_x u + \xi_y v)\rho\omega\end{bmatrix}$$

$$\hat{F}_t = J^{-1}\begin{bmatrix}(\eta_x u + \eta_y v)\rho k \\ (\eta_x u + \eta_y v)\rho\omega\end{bmatrix}$$

$$\hat{E}_{tv} = J^{-1}\begin{Bmatrix}\frac{1}{\rho}(\mu + \sigma^*\mu_T)\left[(\xi_x^2 + \xi_y^2)\frac{\partial(\rho k)}{\partial \xi} + (\xi_x\eta_x + \xi_y\eta_y)\frac{\partial(\rho k)}{\partial \eta}\right] \\ \frac{1}{\rho}(\mu + \sigma\mu_T)\left[(\xi_x^2 + \xi_y^2)\frac{\partial(\rho\omega)}{\partial \xi} + (\xi_x\eta_x + \xi_y\eta_y)\frac{\partial(\rho\omega)}{\partial \eta}\right]\end{Bmatrix}$$

$$\hat{F}_{tv} = J^{-1}\begin{Bmatrix}\frac{1}{\rho}(\mu + \sigma^*\mu_T)\left[(\eta_x^2 + \eta_y^2)\frac{\partial(\rho k)}{\partial \eta} + (\xi_x\eta_x + \xi_y\eta_y)\frac{\partial(\rho k)}{\partial \xi}\right] \\ \frac{1}{\rho}(\mu + \sigma\mu_T)\left[(\eta_x^2 + \eta_y^2)\frac{\partial(\rho\omega)}{\partial \eta} + (\xi_x\eta_x + \xi_y\eta_y)\frac{\partial(\rho\omega)}{\partial \xi}\right]\end{Bmatrix}$$

$$\hat{H}_t = J^{-1}\begin{bmatrix}PP - \beta^*\rho\omega k \\ \alpha\frac{\omega}{k}pp - \beta\rho\omega^2\end{bmatrix}, \qquad PP = \tau_{ij}\frac{\partial u_i}{\partial x_j}$$

where J is the Jacobian of transformation, $J = \partial(x, y)/\partial(\xi, \eta)$.

Rearranging terms in Eq. (6) results in the set of equations

$$\frac{\partial \hat{Q}_t}{\partial \tau} + \frac{\partial}{\partial \xi}(\hat{E}_t - Re^{-1}\hat{E}_{tv}) + \frac{\partial}{\partial \eta}(\hat{F}_t - Re^{-1}\hat{F}_{tv}) = \hat{H}_t \qquad (7)$$

The linearization for flux and source terms of the previous equations results in the set of equations

$$(\hat{E}_t - Re^{-1}\hat{E}_{tv})^{n+1} \approx (\hat{E}_t - Re^{-1}\hat{E}_{tv})^n + \left(\frac{\partial \hat{E}_t}{\partial \hat{Q}_t} - Re^{-1}\frac{\partial \hat{E}_{tv}}{\partial \hat{Q}_t}\right)\Delta\hat{Q}_t + \mathbb{O}(\Delta\tau)^2$$

$$(\hat{F}_t - Re^{-1}\hat{F}_{tv})^{n+1} \approx (\hat{F}_t - Re^{-1}\hat{F}_{tv})^n + \left(\frac{\partial \hat{F}_t}{\partial \hat{Q}_t} - Re^{-1}\frac{\partial \hat{F}_{tv}}{\partial \hat{Q}_t}\right)\Delta\hat{Q}_t + \mathbb{O}(\Delta\tau)^2$$

$$\hat{H}_t^{n+1} \approx \hat{H}_t^n + \frac{\partial \hat{H}_t}{\partial \hat{Q}_t}\Delta\hat{Q}_t + \mathbb{O}(\Delta\tau)^2$$

where

$$\Delta\hat{Q}_t = \hat{Q}_t^{n+1} - \hat{Q}_t^n$$

Substituting the previous equations into Eq. (7) yields the delta form of the equations

$$\left[\frac{I}{\Delta\tau} + \delta_\xi\left(\frac{\partial \hat{E}_t}{\partial \hat{Q}_t} - Re^{-1}\frac{\partial \hat{E}_{tv}}{\partial \hat{Q}_t}\right) + \delta_\eta\left(\frac{\partial \hat{F}_t}{\partial \hat{Q}_t} - Re^{-1}\frac{\partial \hat{F}_{tv}}{\partial \hat{Q}_t}\right) - \frac{\partial \hat{H}_t}{\partial \hat{Q}_t}\right]\Delta\hat{Q}_t = -\delta_\xi(\hat{E}_t - Re^{-1}\hat{E}_{tv})^n - \delta_\eta(\hat{F}_t - Re^{-1}\hat{F}_{tv})^n + \hat{H}_t^n \qquad (8)$$

Employing the approximate factorization method, Eq. (8) transforms into the following two equations:

$$\left[I + \Delta\tau\delta_\xi\left(\frac{\partial \hat{E}_t}{\partial \hat{Q}_t} - Re^{-1}\frac{\partial \hat{E}_{tv}}{\partial \hat{Q}_t}\right)\right]\Delta\hat{Q}_t^* = \Delta\tau[\hat{H}_t^n - \delta_\xi(\hat{E}_t - Re^{-1}\hat{E}_{tv})^n - \delta_\eta(\hat{F}_t - Re^{-1}\hat{F}_{tv})^n] \qquad (9)$$

$$\left[I + \Delta\tau\delta_\eta\left(\frac{\partial \hat{F}_t}{\partial \hat{Q}_t} - Re^{-1}\frac{\partial \hat{Q}_{tv}}{\partial \hat{Q}_t}\right) - \frac{\partial \hat{H}_t}{\partial \hat{Q}_t}\right]\Delta\hat{Q}_t = \Delta\hat{Q}_t^* \qquad (10)$$

$$\frac{\partial \hat{E}_t}{\partial \hat{Q}_t} = \begin{bmatrix}\xi_x u + \xi_y v & 0 \\ 0 & \xi_x u + \xi_y v\end{bmatrix}$$

$$\frac{\partial \hat{F}_t}{\partial \hat{Q}_t} = \begin{bmatrix} \eta_x u + \eta_y v & 0 \\ 0 & \eta_x u + \eta_y v \end{bmatrix}$$

$$\frac{\partial \hat{H}_t}{\partial \hat{Q}_t} = \begin{bmatrix} -2\beta^* \omega & 0 \\ 0 & -2\beta\omega \end{bmatrix}$$

For flux terms of Eqs. (9) and (10), backward difference is used if the contravariant velocity U along the ξ direction or the contravariant velocity V along the η direction is positive. Forward difference is used if U or V is negative. The U and V are defined as

$$U = \xi_x u + \xi_y v \qquad V = \eta_x u + \eta_y v$$

Central difference is used to evaluate diffusion terms. The k-ω transport equations have then been transformed into the forms of Eqs. (9) and (10). Solving the system of the discretized equations gives the k and ω quantities on each grid point.

IV. Results and Discussion

A. Fully Turbulent Flow past a Flat Plate

The airflow conditions are Ue = 33 m/s, Te = 294 K, Pe = 1 atm, and Q_{tur} (turbulence intensity) = 0.25%. There is no pressure gradient in the flowfield. The experiment was conducted by Wieghardt and Tillmann and the experimental data are listed in Coles and Hirst.[14] The referenced length is taken as a unit inch. The computation domain is $-20 \leq x \leq 120$ and $0 \leq y \leq 5$. The leading edge of the flat plate is located at $x = 0$. The grid is clustered in the x direction near the leading edge. In the y direction, the grid is clustered, with the first grid point 10^{-4} distance away from the wall.

The Navier–Stokes equations and the k-ω two-equation model are solved in the entire domain. The calculations are performed with an adiabatic wall condition. The inlet freestream ω is set equal to 100. Three grid systems were tested, namely 140 × 31, 140 × 41, and 140 × 51. Figure 1 shows the computed local skin friction coefficient along the plate. The skin friction coefficient C_f is defined by

$$C_f = \tau_w/(1/2\rho_e U_e^2) \tag{11}$$

where τ_w is the shear stress on the wall; ρ_e and U_e are the density and velocity at the edge of the boundary layer. It clearly shows the dependence of the solution on the grid systems. An asymptotic solution, however, can be obtained by using the 140 × 51 grid system. The original k-ω model and the modified model for flow transition are both tested. The computed C_f distributions are revealed to be nearly identical. This is because the flow is fully turbulent starting at the leading edge of the plate. We also tested three different values of ω, i.e., 100, 200, and 300. No distinct difference is observed in the computed C_f distributions. The influence of the freestream values of ω on the C_f is rather weak for the fully turbulent flat plate flow. Three different values of k_R^+, i.e., 5.0, 2.5, and 1.0 are also employed to investigate their effect on the C_f. An insignificant difference is observed in the computed C_f distributions. This confirmed the Wilcox[10] statement in which the k_R^+ value should be less than 5.0 to ensure a smooth surface.

B. Transitional Flow Simulation on a Flat Plate

The experiment of a transitional airflow over a flat plate was investigated by Schubauer and Klebanoff.[15] The inflow conditions are Ue = 24.3 m/s, Te = 293 K, Pe = 1 atm, and Q_{tur} (turbulence intensity) = 0.03%. The modified k-ω model is used in the calculation. The computational domain is $0 \leq x \leq 3$ m and $0 \leq y \leq 0.13$ m. The grid system is 101 × 51. Several values of ω_∞ at the inflow are also tested in the computation. Computed results have been tested to be grid independent. Figure 2 shows comparisons of the computed skin friction distributions, Dey and Narasimha's results,[16] and the experimental data.[15] It clearly shows that the onset of the transitional point is well predicted by the k-ω model in the case of inflow ω_∞ = 100. It is observed that larger value of the ω_∞ delays the transition and smaller value of ω_∞ results in earlier transition. The proper choice of the ω_∞ value has a profound effect on the predicted location of the transition point. It is interesting to note that ω_∞ = 100 is in the order of $10U_e/L$, where L should be the length of the region in the wind tunnel that produces homogeneous isotropic turbulence prior to the test section.

Figure 3 shows the production ($Re^{-1}\tau_{ij}\partial u_i/\partial u_j$) and dissipation ($\beta^*\rho k\omega$) distributions in turbulent kinetic energy equations for the case of inflow ω_∞ = 100. At the onset of transition, the laminar flow turns into unstable state. The production and dissipation are almost zero at this stage. While the fluid flows downstream, both the production and dissipation grow up. The growing rate of the production is higher than the dissipation rate during the transition. Eventually, the production and dissipation reach a balance, shown as a solid line in Fig. 3. After

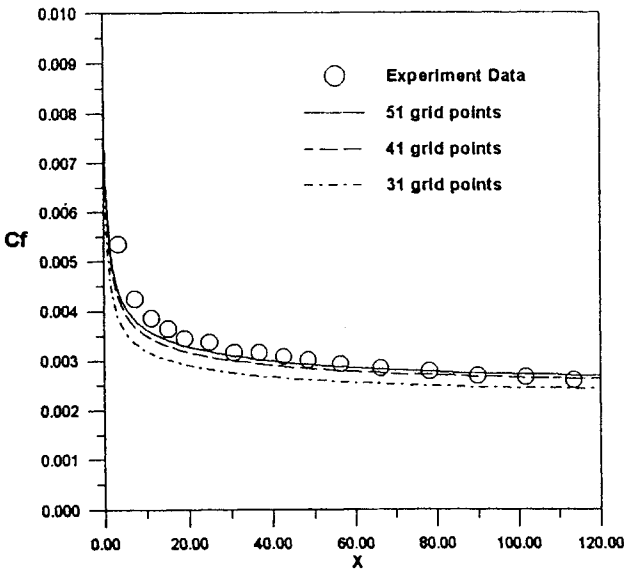

Fig. 1 Skin friction distributions of the fully turbulent flow on a flat plate with different grid points.

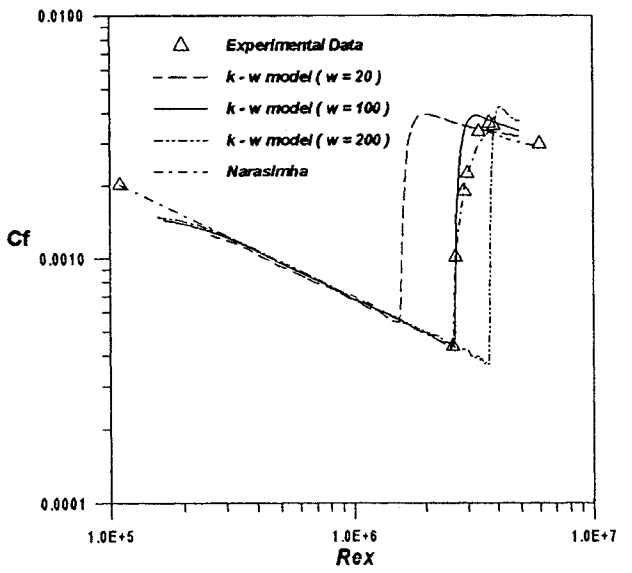

Fig. 2 Skin friction distributions of a transitional flow on a flat plate with freestream turbulence intensity 0.03%.

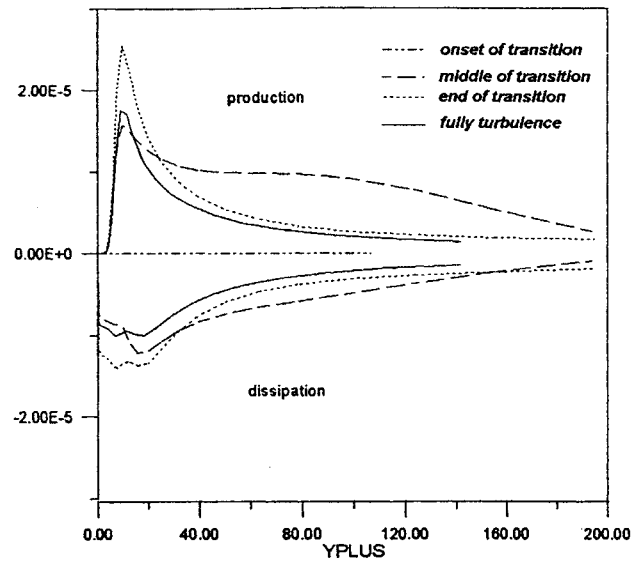

Fig. 3 Production and dissipation distributions in the turbulent kinetic energy equation.

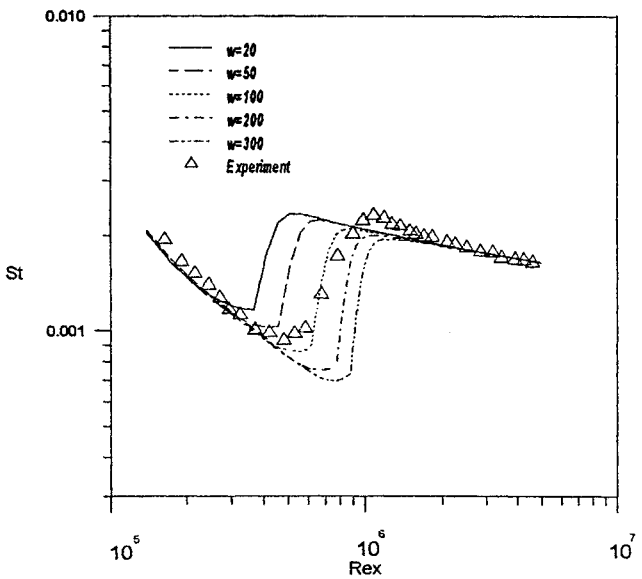

Fig. 4 Effect of specific dissipation rate for the predictions of the onset of transition on the flat plate.

reaching a balance, the transition process is finished. The flow then becomes fully turbulent.

C. Heat Transfer Prediction on a Flat Plate in Flow Transition

The heat transfer experiment conducted by Blair and Werle[17] is simulated by the k-ω model. The air flows over a flat plate with the freestream condition U_e = 30 m/s, ρ_e = 1.16 kg/m^3, T_e = 295 K, and P_e = 1 atm. There is an unheated length of 0.043 m at the leading edge of the flat plate, and a constant wall heat flux of 540 W/m^2 at the rest of the area. The computational domain and grid point are taken as being the same as the previous case. The computed St distributions are shown in Figs. 4 and 5. The St is defined as

$$St = \frac{q_w}{\rho_e C_p U_e (T_{aw} - T_e)} \tag{12}$$

where q_w is the heat flux per unit area on the flat plate, and ρ_e, U_e, and T_e are the density, velocity, and temperature at the edge of the boundary layer, respectively. The specific heat is Cp. The adiabatic wall temperature is T_{aw}. Figure 4 presents

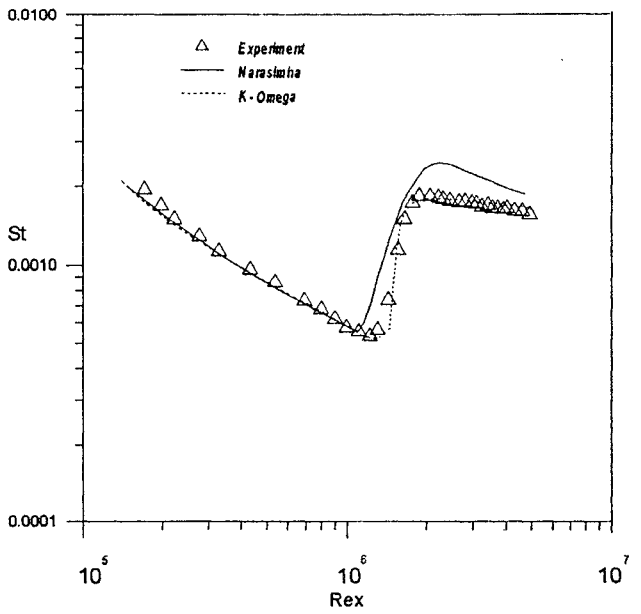

Fig. 5 Heat transfer distributions of a transitional flow on a heated flat plate with turbulence intensity 0.25%.

the results for the case of the freestream Q_{tur} = 1% with various values of inflow ω_∞. It shows that ω_∞ = 100 gave a good prediction in the heat transfer distributions. It again demonstrates the evidence of the proper choice for the ω_∞ value. Figure 5 shows a comparison between the experimental data, results predicted by the modified k-ω model and those by the Dey and Narasimha[16] for the case of the freestream Q_{tur} = 0.25%. It shows that the model (with inflow ω_∞ = 100) predicts excellent heat transfer distribution during the flow transition.

D. Pressure Distributions on Turbine Blade Surface

In this section, we focus on the study of the flow over a two-dimensional turbine blade as shown in Fig. 6. The grid system consists of an outer H grid along the streamwise direction and an inner O grid wrapped around the blade surface. The inner region has 101 × 31 number of grid points and the outer region has a value of 90 × 31. Therefore, there are 73 grid points between the blade passage. The first grid space is normal to the blade surface with a distance of 10^{-4} of a referenced length, which makes the $y^+ < 3$. The referenced length is 2.54 cm. These blades are the first stator of the large-scale rotating turbine model.[18] The inflow conditions are M = 0.0704, $Re = 4.2 \times 10^4$, based on the referenced length. Pressure coefficient Cp is defined as

$$Cp = \frac{P - P2}{P01 - P2}$$

P is the pressure on the blade surface, $P01$ is the total pressure at the inlet, and $P2$ is the static pressure at the exit.

The computed pressure distributions are shown in Fig. 7. The solid and dash lines are the predictions of the k-ω and Baldwin–Lomax models. Experiment data[18] are represented by the symbols. This figure indicates that the results of both models are very close to the experimental data. The upper and lower parts of the closed line represent the pressure coefficients on the pressure side and the suction side, respectively. On the pressure side, from the leading edge to the trailing edge, the flow is accelerated smoothly because of a decrease in Cp in proper order. Nevertheless, on the suction side, near the leading edge, Cp drops abruptly. It is followed by a decrease, then an increase to the trailing edge. Therefore, there is an overspeed near the leading edge followed by an acceleration to the throat. The flow then is decelerated smoothly to the trailing edge.

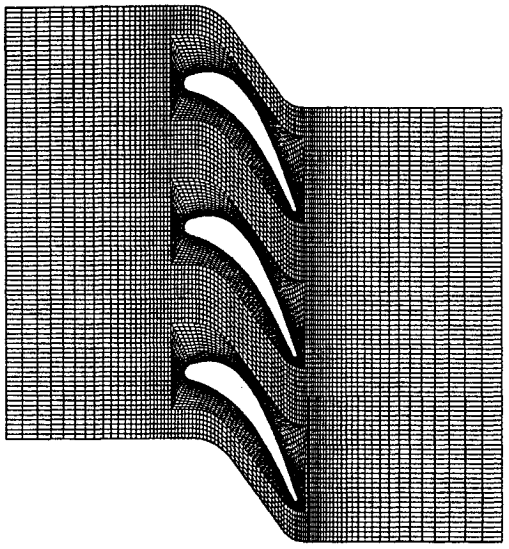

Fig. 6 Grid points of the turbine blades.

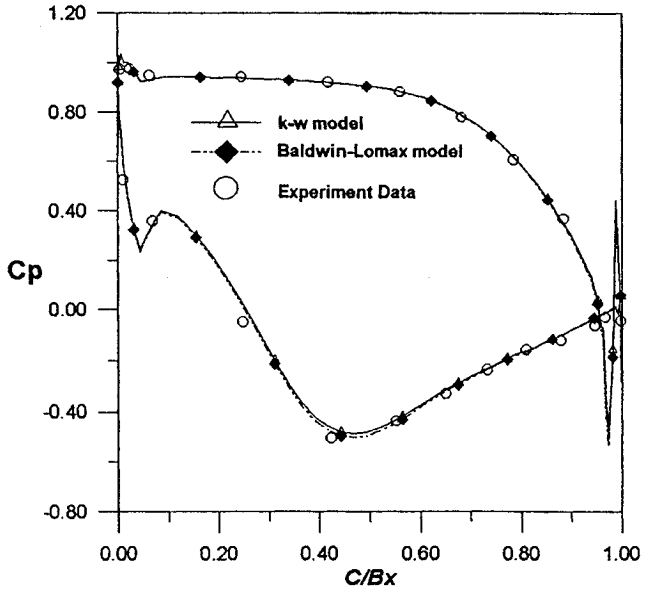

Fig. 7 Pressure distributions on the turbine blade.

E. Heat Transfer Distributions on Turbine Blade Surface

In this section, we focus on the study of the heat transfer distributions of the turbine blade flow. The St is defined by Eq. (12) with a replacement of $T_a - T_w$ for $T_{aw} - T_e$ in the denominator, where q_w is the heat flux per unit area on the blade, ρ_e and U_e are the density and relative velocity at the exit, respectively, Cp is specific heat, T_a is the surface temperature obtained by an adiabatic wall calculation, and T_w is set to be $0.9T_a$. Note that the defined St is insensitive to the values specified for the surface temperature T_w.

1. Heat Transfer Predictions Using the Original k-ω Model

The St distributions on the turbine blade surface are shown in Fig. 8. The solid and dash lines represent the predicted results of the k-ω and Baldwin–Lomax models, respectively. The solid and hollow points are the heat transfer distributions of the experimental data[18] based on the turbulence intensity of 9.8% (grid-in case) and 0.5% (grid-out case), respectively. The current simulation focuses on the case of turbulence intensity 0.5% (i.e., grid-out case). The pressure side is in the area in which C/Bx lies between 0 and -1 and that for the suction side is between 0 and 1. The leading edge is at the location where C/Bx equals 0, and the trailing edge at C/Bx equals 1

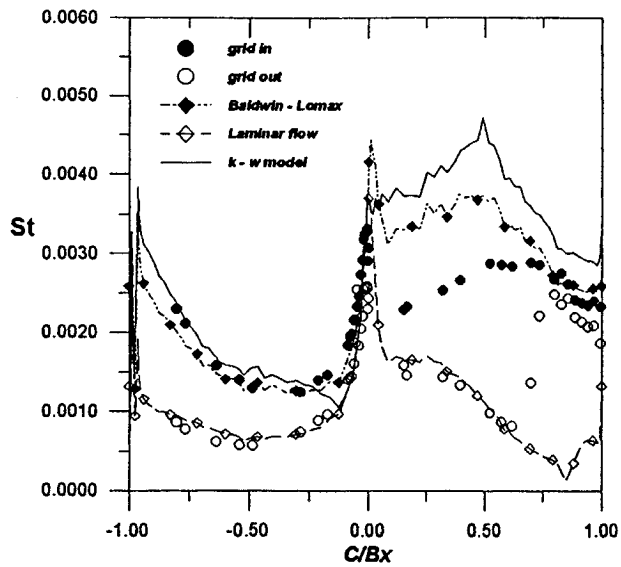

Fig. 8 Heat transfer distributions on the turbine blade with the original k-ω model.

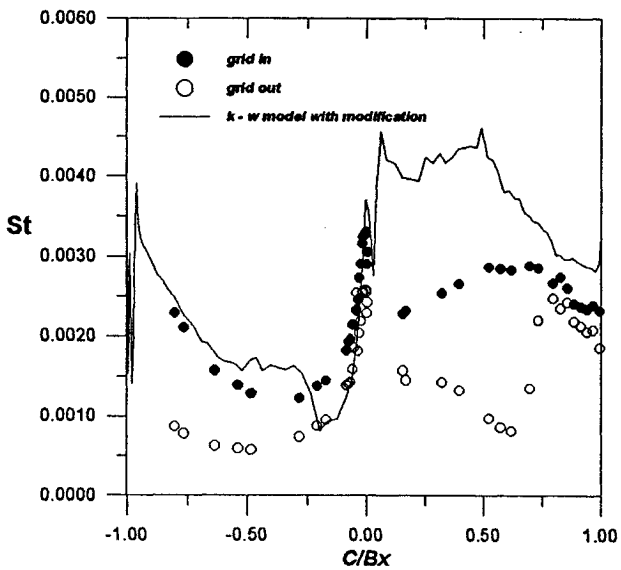

Fig. 9 Heat transfer distributions on the turbine blade with the modified k-ω model.[10]

or -1. On the pressure side, the computed results of the k-ω and Baldwin–Lomax models are close to the experimental data for the grid-in case. However, on the suction side, there are some disparities between the experimental data and the results. Both the k-ω and Baldwin–Lomax models predict that, on the suction side, the flowfield becomes fully turbulent while the fluid flows into the blade. On the pressure side, the flow is still in a laminar state initially, then transition occurs while C/Bx approximate -0.1, followed by the fully turbulent state. For the grid-out experiment data, the flow is laminar on the pressure side, and the flow is still laminar on the suction side initially. Then transition occurs while C/Bx is close to 0.7. Hence, the original k-ω model, without low Re modifications, predicts the onset of the transition much too early. We also compute the heat transfer coefficients based on the laminar flow condition of the turbine blade. The computed results are very close to the grid-out experimental data, excluding the section of the transition on the suction side.

2. Heat Transfer Predictions Using the Modified k-ω Model

The computed results are shown in Fig. 9. The results indicated that the flow is laminar initially on the suction side.

Then transition occurs while C/Bx is close to 0.08, followed by fully turbulent state. On the pressure side, the flowfield is laminar while the fluid flows into the blade. Then transition occurs as C/Bx approximates -0.2. Consequently, the modified k-ω model also predicts the onset of the transition much too early. However, the results have improved slightly in comparison with the predictions of the original k-ω model.

The Wilcox[10] modifications of the k-ω model are in accordance with the transition for the flat plate flows. Therefore it is necessary to modify the k-ω model further to apply the model to flows with surface curvature effects. Because the onset of transition depends on the value of β^*/α^*, revising the value of α^* may delay the transition and ameliorate the problem of early occurrence of transition. In Fig. 10, the transition has been delayed gradually, while $\alpha_0^* = 1/40$ and R_k varies from 15 to 18. As $R_k = 16.5$, the revised model can almost predict the transition correctly. To demonstrate the applicability of the model, the high-turbulence intensity case (grid-in case with $Q_{tur} = 9.8\%$) is computed by using the revised model constants. The computed St distribution is also plotted in Fig. 10. In general, the model produces acceptable solutions within

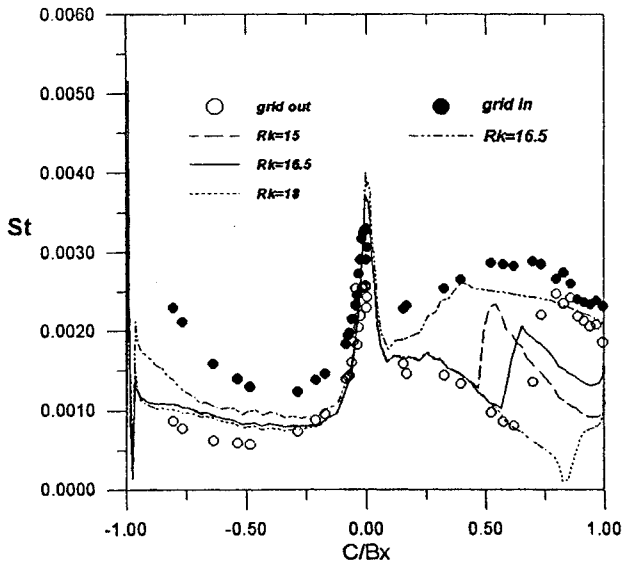

Fig. 10 Heat transfer distributions on the turbine blade revising the value of R_k.

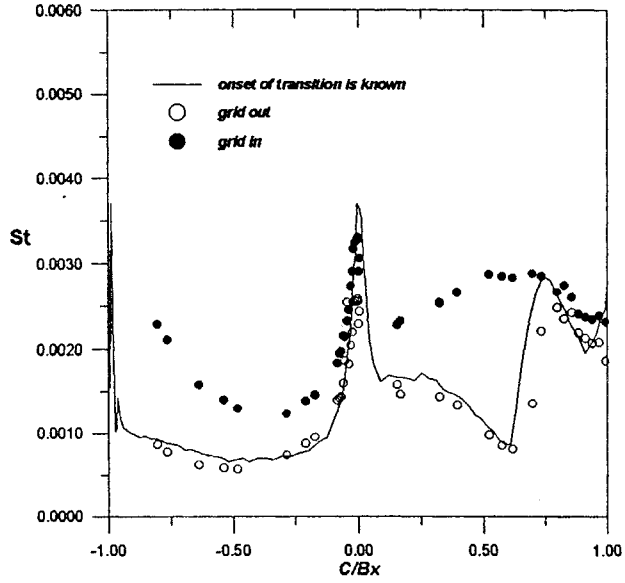

Fig. 11 Heat transfer distributions on the turbine blade with the management of specification the onset of transition.

engineering accuracy for both low- and high-tubulence intensity transitional turbine blade heat transfer problems.

3. Heat Transfer Predictions If the Location of Transition Point Is Specified

For the grid-out experiment case, the flow is laminar on the pressure side. The flow is laminar initially on the suction side, then transition occurs and ends as C/Bx is close to 0.7 and 0.8, respectively. Hence, for the eddy viscosity, we make the management as follows:

$$\mu_{\text{total}} = \mu_{\text{laminar}} + \gamma\mu_T$$

The section of laminar flow on pressure and suction sides $(-1 \le C/B_x \le 0.7)$: Let

$$\gamma = 0$$

Hence

$$\mu_{\text{total}} = \mu_{\text{laminar}}$$

The section of transition process on the suction side $(0.7 < C/B_x \le 0.8)$: Let

$$\gamma = \sin[(x - x_1)/\Delta x](\pi/2)$$

Hence

$$\mu_{\text{total}} = \mu_{\text{laminar}} + \sin[(x - x_1)/\Delta x](\pi/2)\cdot\mu_T$$

where x_1 and x_2 are the locations of the onset and endpoints of the transition process, $\Delta x = x_2 - x_1$. This description is analogous to Narasimha's intermittency concept.[16]

The section of fully turbulence on the suction side $(0.8 < C/B_x)$: Let

$$\gamma = 1$$

Hence

$$\mu_{\text{total}} = \mu_{\text{laminar}} + \mu_T$$

In Fig. 11 the predictions of heat transfer are very close to the experiment data by means of the management made previously. The major disadvantage of this management is that it is required to specify the onset and endpoints of the transition process in advance.

V. Conclusions

This study presents computations using k-ω models for fully turbulent flat plate flow, transitional flat plate flows, and transitional turbine blade flows. For fully turbulent flat plate flow, the k-ω model predicts well the skin friction distributions. The effect of freestream ω_∞ has nearly no effect on the skin friction distributions. For the transitional flat plate flows, the k-ω model predicts well the onset point of the transition with a proper value of ω_∞. The values may be specified as $\mathcal{O}(10U_\infty/L)$. Larger values of ω_∞ may delay the onset point of the transition.

For the pressure distribution on turbine blade, the results of k-ω and Baldwin–Lomax models are very close to the experiment data. The k-ω model could predict accurately the pressure distributions on turbine blade. For the heat transfer distributions, on the pressure side, the results of the original k-ω and Baldwin–Lomax models are close to the experimental data. However, on the suction side, the original k-ω and Baldwin–Lomax models predict the onset of the transition much too early in comparison with the experimental data. The modified k-ω model also predicts the onset of the transition too early, but the results have improved slightly in comparison with the predictions of the original k-ω model. For the turbine

blade flow, it is necessary to take into account the surface curvature effect on α^* and revise the value of α^* to delay the transition and accurately predict the onset point of the transition. This fact has been successfully demonstrated for both low- and high-turbulence intensity transitional flows. The management for the specification of the onset point of the transition could predict heat transfer distributions on turbine blade accurately. The limitation of the management for engineering analysis is that it is difficult to specify the onset and endpoints of the transition process, except those flows known from experiments.

Acknowledgments

This study was supported by the National Science Council of the Republic of China under Grants NSC-83-0401-E-006-010 and NSC-84-2212-E-006-073.

References

[1]Dorney, D. J., and Davis, R. L., "Navier-Stokes Analysis of Turbine Blade Heat Transfer and Performance," *Journal of Turbomachinery*, Vol. 114, Oct. 1992, pp. 796–806.

[2]Hah, C., "A Navier-Stokes Analysis of Three-Dimensional Turbulent Flows Inside Turbine Blade Rows at Design and Off-Design Conditions," *Journal of Engineering for Gas Turbines and Power*, Vol. 106, No. 2, 1984, pp. 421–429.

[3]Rai, M. M., "Three-Dimensional Navier-Stokes Simulations of Turbine Rotor/Stator Interaction," *Journal of Propulsion and Power*, Vol. 5, No. 3, 1989, pp. 305–319.

[4]Hwang, C. J., and Liu, J. L., "Analysis of Steady and Unsteady Turbine Cascade Flows by a Locally Implicit Hybrid Algorithm," American Society of Mechanical Engineers, Paper 92-GT-127, 1992.

[5]Yang, R.-J., Weinberg, B. C., Shamroth, S. J., and McDonald, H., "Numerical Solution of the Navier-Stokes Equations for Two- and Three-Dimensional Turbine Cascades with Heat Transfer," NASA CR-174828, July 1985; also *Journal of Engineering for Gas Turbines and Power*, Vol. 108, Jan. 1986, pp. 93–102.

[6]Yang, R.-J., and Lin, S.-J., "Numerical Solution of Two-Dimensional Multistage Rotor/Stator Unsteady Flow Interactions," *Journal of Propulsion and Power*, Vol. 10, No. 6, 1994, pp. 876–883.

[7]Boyle, R. J., "Navier-Stokes Analysis of Turbine Blade Heat Transfer," *Journal of Turbomachinery*, Vol. 113, July 1991, pp. 392–403.

[8]Schmidt, R. C., and Patankar, S. V., "Simulating Boundary Layer Transition with Low-Reynolds Number k-ε Turbulence Models: Part 1 and Part 2," *Journal of Turbomachinery*, Vol. 113, Jan. 1991, pp. 10–26.

[9]Wilcox, D. C., "Comparison of Two-Equation Turbulence Models for Boundary Layers with Pressure Gradient," *AIAA Journal*, Vol. 31, No. 8, 1993, pp. 1414–1421.

[10]Wilcox, D. C., "Turbulence Modeling for CFD," DCW Industries Inc., La Canada, CA, 1993.

[11]Menter, F. R., "Influence of Freestream Values on k-ω Turbulence Model Predictions," *AIAA Journal*, Vol. 30, No. 6, 1992, pp. 1657–1659.

[12]Rai, M. M., "Navier-Stokes Simulations of Rotor-Stator Interaction Using Patched and Overlaid Grids," *Journal of Propulsion and Power*, Vol. 3, No. 5, 1987, pp. 387–396.

[13]Rai, M. M., and Chakravarthy, S. R., "An Implicit Form for the Osher Upwind Scheme," *AIAA Journal*, Vol. 24, No. 5, 1986, pp. 735–743.

[14]Coles, P., and Hirst, E. (eds.), *Proceedings and Computation of Turbulent Boundary Layers—1968 AFOSR-IFP Stanford Conference*, Vol. 2, Stanford Univ., Stanford, CA, 1968.

[15]Schubauer, G. B., and Klebanoff, P. S., "Contributions on the Mechanics of Boundary-Layer Transition," NASA TN 3489, 1955.

[16]Dey, J., and Narasimha, R., "An Integral Method for the Calculation of 2D Transitional Boundary Layers," Dept. of Aerospace Engineering, Indian Inst. of Science, Rept. 88 FM 7, Bangalore, India, 1988.

[17]Blair, M. F., and Werle, M. J., "Combined Influence of Free-Stream Turbulent and Favorable Pressure Gradients on Boundary Layer Transition and Heat Transfer," United Technologies Research Center, Rept. R81-914388-17, March 1981.

[18]Dring, R. P., Blair, M. F., Joslyn, H. D., and Verdon, J. M., "The Effects of Inlet Turbulence and Rotor/Stator Interactions on the Aerodynamics and Heat Transfer of a Large-Scale Rotating Turbine Model," NASA CR 4079, May 1986.